

Crystal structure and improved antisense properties of 2'-O-(2-methoxyethyl)-RNA

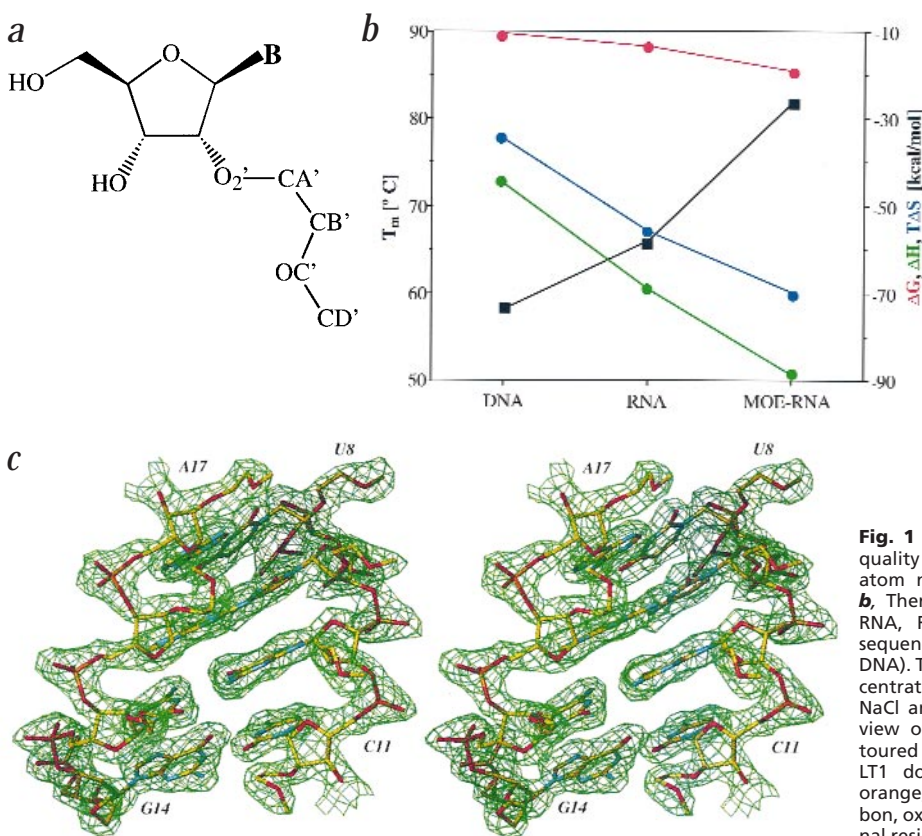
Marianna Teplova¹, George Minasov¹, Valentina Tereshko¹, Gopal B. Inamati², P. Dan Cook², Muthiah Manoharan² and Martin Egli¹

¹Department of Molecular Pharmacology and Biological Chemistry and The Drug Discovery Program, Northwestern University Medical School, Chicago, Illinois 60611, USA. ²Department of Medicinal Chemistry, Isis Pharmaceuticals Inc., Carlsbad, California 92008, USA.

2'-O-(2-Methoxyethyl)-RNA (MOE-RNA) is a nucleic acid analog with promising features for antisense applications. Compared with phosphorothioate DNA (PS-DNA), the MOE modification offers improved nuclease resistance, enhanced RNA affinity, improved cellular uptake and intestinal absorption, reduced toxicity and immune stimulation. The crystal structure of a fully modified MOE-RNA dodecamer duplex (CGCGAAUUCGCG) was determined at 1.7 Å resolution. In the majority of the MOE substituents, the torsion angle around the ethylene alkyl chain assumes a *gauche* conformation. The conformational preorganization of the MOE groups is consistent with the improved RNA affinity and the extensive hydration of the substituents could play a role in the improved cellular uptake of MOE-RNA. A specific hydration pattern that bridges substituent and phosphate oxygen

atoms in the minor groove of MOE-RNA may explain its high nuclease resistance.

Chemical modification of oligonucleotides has yielded second generation analogs that combine high RNA affinity and pairing specificity, and are both chemically more stable and more resistant to nuclease degradation than DNA or RNA¹⁻³. Such compounds may be suitable as antisense oligonucleotides (AS-ONs) in the treatment of a host of diseases, including cancer, inflammation and viral infections. For example, certain 2'-O-alkoxyalkyl ONs display promising properties for *in vivo* applications^{4,5}. Among them, MOE-RNA (Fig. 1a) shows strong self-pairing (Fig. 1b) and forms duplexes with RNA that are 2 °C more stable on average per modification than the corresponding PS-DNA-RNA hybrids⁴⁻⁷. The higher RNA affinity is accompanied by a significantly enhanced protection against nuclease degradation, rivaling or surpassing that of PS-DNA^{3,6}. Both features could help overcome the current pharmacodynamic, pharmacokinetic and toxicologic limitations encountered with phosphorothioate oligodeoxynucleotides (PS-ODNs)⁸. Thus, favorable RNA hybridization and less PS content may allow reduced dosing frequencies and permit the use of shorter AS-ONs⁹. Higher stability of the AS-ON-RNA complex can lead to RNase H-independent downregulation of the targeted message through a steric block mechanism¹⁰. In addition, such AS-ONs might improve the chances for future oral administration of antisense-therapeutics¹¹, and a reduction of the number of PS-linkages with retained or enhanced nuclease resistance should lead to decreased immune stimulation and toxicity¹²⁻¹⁷. To better define the origins of the promising antisense properties displayed by MOE-RNA, we have determined high-resolution crystal structures of a completely MOE-modified RNA duplex, the first for an RNA molecule carrying a chemical modification on every residue.



Overall features of the duplex
Four structures of the MOE-RNA dodecamer duplex were determined, based on crystals grown under different conditions and using data collected at room temperature and 120 K (RT and LT1 to 3, Table 1). In all four structures the conformations of the MOE substituents on the surface of the duplex were well defined as manifested by sum electron density maps surrounding the final models (Fig. 1c). The MOE-RNA duplex has a low helical rise of

Fig. 1 Structure and stability of MOE-RNA and quality of the electron density. **a**, Structure and atom numbering of the MOE-RNA nucleoside. **b**, Thermodynamic stability of self-paired MOE-RNA, RNA and DNA oligonucleotides of the sequence CGCGAAUUCGCG (T instead of U in DNA). The T_m s were measured at 4 mM strand concentration in 10 mM Tris-HCl pH 7.0 and 150 mM NaCl and ΔG° was calculated at 37 °C. **c**, Stereo view of the $2F_o - F_c$ sum electron density (contoured at 1 σ) around the terminal region of the LT1 dodecamer structure. Atoms are colored orange, yellow, red and cyan for phosphorus, carbon, oxygen and nitrogen, respectively, and terminal residues are labeled.

letters

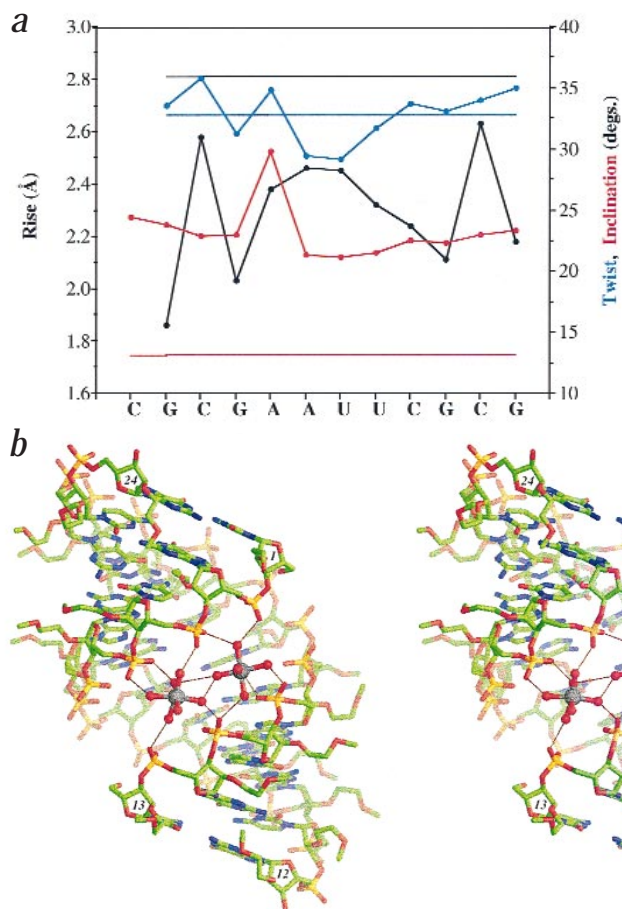


Fig. 2 Geometry and topology of the MOE-RNA duplex. **a**, Helical rise (black), twist (blue) and inclination (red) values for individual base pairs in the LT1 MOE-RNA duplex, calculated with the program CURVES³⁶. Straight lines indicate the corresponding values for standard A-form RNA. **b**, Stereo view of the overall conformation of the LT3 MOE-RNA dodecamer duplex and the Mg²⁺ ions bound in its major groove. The Mg²⁺ hexahydrate complex on the left is located on the crystallographic dyad. Atoms are colored gray, orange, red, green and blue for magnesium, phosphorus, carbon, oxygen and nitrogen, respectively. Hydrogen bonds are solid black lines and terminal residues are labeled. **c**, Molecular surface representation of the MOE-RNA LT2 duplex, viewed into the minor groove. Atoms of phosphate groups and MOE substituents are colored orange and green, respectively, and all others are colored light gray.

~2.2 Å, roughly 0.5 Å below that of standard A-form RNA¹⁸ (Fig. 2a). This axial compression of the double helix neither affects its diameter (24 Å) nor the position of the helical axis and the number of repeats per turn (11, average helical twist 33°, Fig. 2a). However, the structure shows strong inclination of base pairs (average 23°, Fig. 2a) and high roll values (average 13°). Despite the non-canonical helix geometry, the structures reveal no irregularities in the conformation of the backbone or sugar moieties. Thus, all 2'-O-modified riboses have the expected C3'-endo pucker. Moreover, low root mean square (r.m.s.) deviations among the six backbone torsion angles attest to the geometric rigidity of the duplex.

In the monoclinic lattice, infinite columns of duplexes cross in a roughly perpendicular manner, whereby the columns form sheets that run more or less normal to the y-axis. The latter are stitched together by Mg²⁺ ions that are located on crystallographic dyads. At the intersections, the major grooves of the duplexes face each other and the Mg²⁺ ions mediate close contacts between phosphate groups from all four strands of adjacent duplexes (Fig. 2b, only one duplex shown). A second fully hydrated Mg²⁺ (hexahydrate) only forms contacts to phosphates of one duplex. Mg²⁺ ions were located in several RNA crystal structures, including tRNA^{Phc} (ref. 19), the P4-P6 domain of a group I intron²⁰ and the hammerhead ribozyme²¹. Although Mg²⁺ binding was frequently found to involve major groove sites, the coordination mode observed in the MOE-RNA structure is unique. Both Mg²⁺ ions are located at the periphery of the major groove and form outer-sphere, water-mediated contacts with phosphate groups but not with base functionalities. Packing

between RNA duplexes such that their minor grooves fit together is much more common than the interaction between major grooves seen here (see refs 20 and 22 for examples).

The Mg²⁺ ion that bridges two duplexes is found in all four structures and appears to be important for lattice formation. Phosphate groups across the deep groove are spaced by merely 2 Å in the MOE-RNA duplex, ~4 Å below that of canonical A-form RNA (Fig. 2b). With no bending apparent, the narrower major groove is a direct result of the axial compression. It is likely that by bridging phosphates from opposite strands and contracting the groove, the Mg²⁺ ion is also at the origin of the observed abnormally low helical rise. It is noteworthy that the narrowing of the major groove observed in the crystal structure of the E loop of 5S rRNA is also believed to be facilitated by four Mg²⁺ ions buried in the major groove²³.

Topology of the minor groove

The different conformations adopted by the individual MOE substituents block access to the bases at the floor of the normally wide and shallow RNA minor groove to various degrees. In some cases, MOE moieties protrude into the minor groove roughly perpendicular to the helix axis (Fig. 2b). However, at other locations, the moieties appear to follow the backbone in a 5' to 3' direction, generating van der Waals contacts to the ribose of an adjacent intra-strand residue (Fig. 2c). In the central part of the duplex, methyl groups of the MOE substituents from residues U7 and U20 are in van der Waals contact (the distance between CD' atoms in LT2 is 4.1 Å). This arrangement effectively seals the minor groove (Fig. 2c). However, despite the irregular spacings

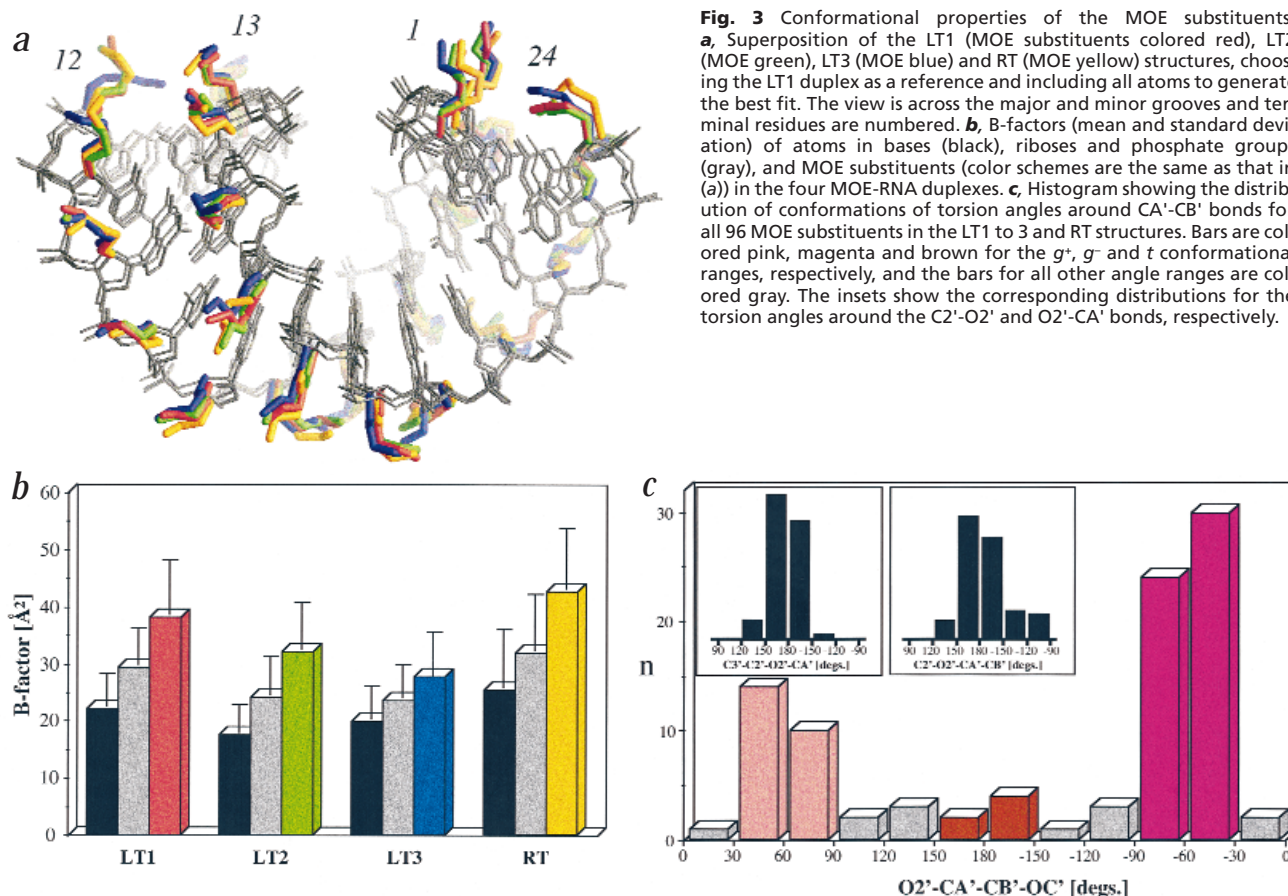


Fig. 3 Conformational properties of the MOE substituents. **a**, Superposition of the LT1 (MOE substituents colored red), LT2 (MOE green), LT3 (MOE blue) and RT (MOE yellow) structures, choosing the LT1 duplex as a reference and including all atoms to generate the best fit. The view is across the major and minor grooves and terminal residues are numbered. **b**, B-factors (mean and standard deviation) of atoms in bases (black), riboses and phosphate groups (gray), and MOE substituents (color schemes are the same as that in (a)) in the four MOE-RNA duplexes. **c**, Histogram showing the distribution of conformations of torsion angles around CA'-CB' bonds for all 96 MOE substituents in the LT1 to 3 and RT structures. Bars are colored pink, magenta and brown for the g^+ , g^- and t conformational ranges, respectively, and the bars for all other angle ranges are colored gray. The insets show the corresponding distributions for the torsion angles around the C2'-O2' and O2'-CA' bonds, respectively.

of MOE substituents along the backbones, no unusual changes in the distances between phosphorus atoms across the MOE-RNA minor groove occur compared with a regular RNA duplex. Thus, the RNA minor groove can accommodate the spatial requirements of the MOE substituents.

Conformation of the MOE substituents

Comparison of the arrangements of individual substituents in the four structures reveals only minor deviations for most residues (Fig. 3a). All crystallographic refinements were carried out without restraining the torsion angles of MOE substituents. Although their mobilities in the crystals exceed those of base and ribose-phosphate backbone atoms (Fig. 3b), the substituents are ordered and exhibit distinct conformational preferences. Most significant among them is the favored g^+ or g^- conformation around the CA'-CB' bond (Figs 1a and 3c). Only two substituents per structure adopt conformations that lie outside these angle ranges. However, it appears that the g^+ and g^- arrangements have different stabilities since g^- occurs roughly twice as often (Fig. 3c). There are no obvious steric reasons for this and lattice interactions are an unlikely cause as well. On the other hand, the reasons for the predominant *trans* orientation of the torsions around the C2'-O2' and O2'-CA' bonds seem to be mainly steric in nature. For residue G3 the *trans* conformation around the CA'-CB' bond is conserved in all four structures, hinting at a lattice contact as the possible origin. Indeed, modeling of g^+ or g^- conformations with MOE of G3 leads to repulsive contacts with a particular MOE substituent of an adjacent duplex. Other residues displaying a *trans* conformation of the MOE substituent are C21 in LT1 and LT2 and

G24 in the LT3 and RT structures. In summary, the structures demonstrate that the geometry of the MOE substituents at least in the double helical state is mainly governed by the stereoelectronic *gauche* effect²⁴ and, to the extent that the tested crystallization conditions have allowed us to probe this, only marginally dependent on pH, temperature and ionic strength.

Hydration and hydrogen bonding interactions

2'-O-MOE substitution of RNA introduces an additional acceptor atom in the minor groove (OC', Fig. 1a). A hydration pattern that is associated with a *gauche* conformation of the substituent is present in several residues (Fig. 4a,b). This pattern involves a water coordinated to OC', O2' and O3', under formation of two bifurcated hydrogen bonds. Either one or two additional water molecules then hydrogen bond to that water. This hydration motif is more common for substituents with a g^- conformation around the ethylene bond. A second water molecule can link the above water to the phosphate group of the same residue when the substituent adopts a g^+ orientation (Fig. 4a,b). For the g^+ arrangement the corresponding distance is slightly too long to be bridged by a single water molecule. It is possible that the water structure around the g^- MOE moiety is energetically favorable relative to the one around substituents with a g^+ conformation, providing a rationale for the higher number of substituents displaying the former geometry. Water molecules can also mediate hydrogen bond interactions between bases and substituents in cases where the latter assume a *trans* conformation. For example, a water molecule links OC' and N2 of residue G24 (Fig. 4c). Therefore, MOE substituents adopting either *gauche* or *trans* conformations can mediate

letters

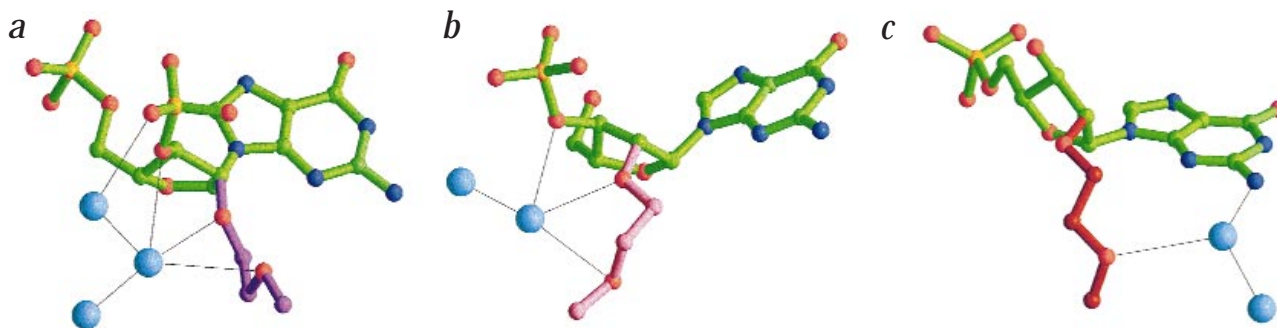


Fig. 4 MOE-mediated hydration of residues with *gauche* and *trans* conformations around the ethyl bond of the 2'-O-substituent. The coloring of MOE carbon atoms corresponds to the conformation around the ethyl bond and matches the color scheme of the histogram in Fig. 3b. **a**, Residue G22 of structure LT1, *g*⁻ conformation. **b**, Residue G2 of structure LT1, *g*⁻ conformation. **c**, Residue G24 of structure LT3, *t* conformation. Atoms are colored orange, green, red and blue for phosphorus, carbon, oxygen and nitrogen, respectively. Water molecules are drawn as large cyan colored spheres and hydrogen bonds are solid black lines.

enthalpically favorable interactions, consistent with the greater enthalpic contribution to MOE-RNA duplex formation relative to unsubstituted RNA (Fig. 1b).

Structural origins of the improved antisense properties

Our structural results are consistent with the higher affinity of MOE-RNA for RNA as compared to DNA. As expected the sugars are locked in the C3'-*endo* conformation, a prerequisite of any RNA mimic. In the case of the 2'-O-alkyl modifications, longer substituents destabilize the duplex formed between the modified strand and the RNA target²⁵. Conversely, conformational preorganization with MOE-RNA includes sugar moiety and substituent, as both are governed by the *gauche* effect, with the unique hydration pattern around MOE substituents providing additional rigidity. Dominance of the MOE geometry by the *gauche* effect is largely borne out by the crystal structures. The results presented here are in line with those of an earlier crystallographic study, revealing adoption of a *gauche* geometry by the three O-C-C-O moieties in a single 2'-O-methyl-[tri(oxyethyl)]-modified thymidine²⁶. Although our structures of double-stranded MOE-RNA cannot provide direct evidence, it is plausible that the observed conformational preferences of the MOE moiety also prevail in the single-stranded state, providing an entropic advantage for pairing. Interestingly, molecular dynamics simulations of a MOE-RNA single strand generated a rigid structure that closely resembles the conformation of the MOE strand in the duplex state²⁷.

A further feature of MOE-RNA established by the crystal structures is the extensive hydration of the minor groove and backbones. Up to three first-shell water molecules can be stabilized by the MOE moiety, assisted by bridging and non-bridging phosphate oxygens. The chelate-like trapping of water molecules between oxygen acceptors of substituent and backbone (Fig. 4 a,b) suggests an important role of water in the overall stability of MOE-RNA. In A-form RNA, the 2'-hydroxyl groups can also stabilize water bridges between sugar and base and sugar and phosphate moieties in the minor groove²⁸. By comparison, the hydra-

tion shells of phosphate groups, sugars and bases overlap only weakly in B-form DNA²⁹.

PS-ODNs showed relatively poor permeability in an *in situ* single-pass perfusion model that was used to assess the absorption of ONs in various segments of the rat intestine³⁰. Conversely, MOE oligoribonucleotides with PO backbones had 2.5- to 10-fold increased permeability relative to PS-ODNs. Paracellular absorption, believed to be the dominant route for uptake of ONs, is influenced by the size, charge and hydrophilicity of an antisense compound and correlates strongly with water flux and intercellular tight junction diameter. The considerably better uptake of MOE-ONs relative to PS-

Table 1 Crystal data and refinement parameters

	LT1 ¹	LT2	LT3	RT ¹
Crystal data				
a (Å)	41.20	41.32	42.00	44.06
b (Å)	34.44	34.55	35.60	35.40
c (Å)	46.62	46.60	47.14	48.34
β (°)	92.4	92.3	93.2	95.0
Data collection				
Source/detector	Synchrotron-APS/MARCCD		Rigaku RU200/R-axis IIc	
Temperature	120 K	120 K	120 K	RT
Total no. of reflections	39,271	24,219	22,518	11,424
No. of unique reflections	7,032	6,889	4,996	2,129
Resolution (Å)	1.70	1.80	1.95	2.70
Completeness (%)	99.4	99.7	97.1	98.0
R _{sym} ² (%)	5.5	6.1	5.8	7.2
Refinement statistics				
No. of RNA atoms	602			
No. of waters	105	111	122	13
No. of Mg ²⁺ ions	1	1	2	2
R.m.s. distances (Å)	0.011	0.009	0.011	0.010
R.m.s. angles (°)	1.89	1.64	1.88	1.68
Mean B, RNA (s.d., Å ²)	22.9 (8.0)	28.1 (8.7)	22.8 (6.5)	31.5 (11.6)
Mean B, water (s.d., Å ²)	30.9 (6.8)	34.9 (7.9)	36.0 (9.9)	31.6 (3.4)
No. of refls. [F>2σ(F)]	6,412	5,532	4,359	1,881
R-factor ³ (work set)	0.206	0.207	0.209	0.193
R-factor ⁴ (test set)	0.258	0.248	0.257	0.252

¹LT, low temperature (120 K); RT, room temperature.

²R_{sym} = $\sum_{hkl} \sum_i |I(hkl)_i - \langle I(hkl) \rangle| / \sum_{hkl} \sum_i \langle I(hkl) \rangle$.

³R-factor = $\sum_{hkl} |F(hkl)_o - F(hkl)_c| / \sum_{hkl} F(hkl)_o$.

⁴For 10% of the data³⁷.

ODNs is likely a consequence of the different backbone polarities and is consistent with the extensive hydration of the MOE substituents.

The precise origins of nuclease resistance are currently not understood. Second generation oligonucleotide modifications can offer improved protection against nuclease degradation compared with PS-DNA. Structural studies that lead to insights concerning the protection mechanism may yield design principles for the development of future modifications. Steric hindrance is a likely cause of the improved resistance observed with MOE-RNA. Thus, a 2'-substituent comprising three ethylene glycol moieties further enhances nuclease resistance⁶. The intricate water network between MOE substituents and bridging and non-bridging phosphate oxygens may enhance steric hindrance. Stably bound water molecules could also interfere with phosphoryl transfer or could alter the reactivity of the phosphodiester moiety. Finally, the lower toxicity of this novel modification relative to PS-DNA may arise from the reduced avidity of MOE-RNA for serum protein binding as a result of its elevated hydration.

Methods

Synthesis, purification and crystallization. The MOE-RNA dodecamer was synthesized on a 10 μ M scale on an Expedite solid phase synthesizer, as described⁶. The oligomer was purified with reverse phase HPLC and ion exchange chromatography. The homogeneity was confirmed by capillary gel electrophoresis and mass spectrometry. Crystallization trials were conducted with the hanging drop vapor diffusion method, equilibrating 4 μ l droplets (2 μ l 4 mM RNA and 2 μ l reservoir) against 1 ml of a reservoir solution. The final concentrations of reservoir components for growing the LT1 to 3 and RT crystals were as follows. LT1: 50 mM Na Hepes, pH 6.2; 50 mM MgCl₂. LT2: 50 mM Na Hepes, pH 7.5; >50 mM MgCl₂. LT3: 50 mM Na Hepes, pH 7.5; 100 mM MgCl₂. RT: 50 mM Na Hepes, pH 7.5; 50-100 mM MgCl₂. The precipitant in all cases was 15% (v/v) PEG400 and the space group was monoclinic C2. Cell constants are listed in Table 1.

Data collection. For the data collections at low temperature, crystals were flash-frozen in a nitrogen stream (120 K) and the room temperature data were collected on a crystal that was sealed in a glass capillary along with a droplet of mother liquor. Data collections were conducted either on the Dupont-Northwestern-Dow Consortium Access Team (DND-CAT) insertion device beamline at sector 5 of the Advanced Photon Source at Argonne National Laboratory (wavelength 0.9780 Å, MARCCD detector) or on an in-house Rigaku RU-200 rotating anode/R-axis Ilc image plate setup (Cu K α radiation, λ = 1.548 Å, Table 1).

Crystal structure determination and refinement. All data were processed and scaled in the DENZO/SCALEPACK program suite³¹ (Table 1). The structure was initially solved with the Molecular Replacement method, using a 2.3 Å resolution LT data set collected in-house (data not shown). The program AMORE³² was used in combination with A-form RNA duplex models whose helical rise values were varied between 2.2 and 2.7 Å. All four structures were refined with program X-PLOR³³, using the most recent nucleic acid geometry parameters³⁴. No torsion angle restraints were used for the MOE substituents. R-factors and r.m.s. deviations for bonds and angles from standard values for the final models are listed in Table 1.

Thermal denaturation studies. Melting temperatures were measured on a Beckman DU-7500 UV spectrophotometer, equipped with a Peltier thermal control unit. Equilibrium melting curves of the DNA, RNA and MOE-RNA 12-mers in buffered solutions with between 2 and 12 μ M concentrations were recorded. The buffer was 10 mM Tris-HCl, pH 7.0, and the NaCl concentration

was 150 mM. The lower temperature limit was 25 °C, the upper temperature limit was 95 °C, and the temperature increment was 0.5 °C with an equilibration time of 1 min. For each dodecamer two separate heating and cooling cycles were conducted and the data were averaged to calculate the T_m values. Thermodynamic parameters were then extracted from 1/T_m vs. ln[C] plots³⁵.

Coordinates. The coordinates and reflection data for the four structures have been deposited in the Nucleic Acid Database (accession codes: AR0015 (LT1), AR0016 (LT2), AR0017 (LT3), and AR0018 (RT)).

Acknowledgments

This work was supported through a grant by the National Institutes of Health to M.E. We are indebted to Northwestern University Medical School for supporting structural research through the Macromolecular Crystallography and Biochemical Computation Resource and to the Northwestern Drug Discovery Program. We thank B. Ross and his group at Isis Pharmaceuticals Inc. for providing the phosphoramidites for the dodecamer synthesis and S.T. Wallace for technical assistance. Part of the data collections were performed at the DuPont-Northwestern-Dow Collaborative Access Team (DND-CAT) Synchrotron Research Center located at Sector 5 of the Advanced Photon Source at Argonne National Laboratory, Argonne, Illinois. DND-CAT is supported by the E.I. DuPont de Nemours & Co., The Dow Chemical Company, the U.S. National Science Foundation and the State of Illinois.

Correspondence should be addressed to M.M. e-mail: mmanohar@isisph.com or M.E. email: m-egli@nwu.edu

Received 30 October, 1998; accepted 8 March, 1999.

- De Mesmaeker, A., Häner, R., Martin, P. & Moser, H. E. *Acc. Chem. Res.* **28**, 366–374 (1995).
- Crooke, S.T. In *Handbook of experimental pharmacology*, vol. 131, *Antisense Research and Applications* (ed. Crooke, S.T.) 1–50 (Springer-Verlag, Berlin and Heidelberg, 1998).
- Cook, P. D. *Annu. Med. Rep. Chem.* **33**, 313–325 (1998).
- Altmann, K.-H. et al. *Biochem. Soc. Trans.* **24**, 630–637 (1996).
- Altmann, K.-H. et al. *Chimia* **50**, 168–176 (1996).
- Martin, P. *Helv. Chim. Acta* **78**, 486–504 (1995).
- Freier, S. M. & Altmann, K.-H. *Nucleic Acids Res.* **25**, 4429–4443 (1997).
- Akhtar, S. & Agrawal, S. *Trends Pharmacol. Sci.* **18**, 12–18 (1997).
- Greig, M. J., Gaus, H., Cummins, L. L., Sasmor, H. & Griffey, R.H. *J. Am. Chem. Soc.* **117**, 10765–10766 (1995).
- Baker, B. F. et al. *J. Biol. Chem.* **272**, 11994–12000 (1997).
- Agrawal, S. *Trends Biotechnol.* **14**, 376–387 (1996).
- Gao, W. Y., Storm, C., Egan, W. & Cheng, Y. C. *Mol. Pharmacol.* **43**, 45–50 (1993).
- Wallace, T. L., Bazemore, S. A., Kornbrust, D. J. & Cossom, P. A. *J. Pharmacol. Exp. Ther.* **278**, 1306–1312 (1996).
- Agrawal, S. et al. *Antisense Nucleic Acid Drug Dev.* **7**, 575–584 (1997).
- Henry, S. P. et al. *Anti-Cancer Drug Design* **12**, 1–14 (1997).
- Henry, S. P., Monteith, D., Bennett, F. & Levin, A. A. *Anti-Cancer Drug Design* **12**, 409–420 (1997).
- Levin, A. A. et al. In *Handbook of experimental pharmacology*, vol. 131, *Antisense research and applications* (ed. Crooke, S.T.) 169–215 (Springer Verlag, Berlin and Heidelberg; 1998).
- Saenger, W. *Principles of nucleic acid structure* (Springer Verlag, New York; 1984).
- Quigley, G. J., Teeter, M. M. & Rich, A. *Proc. Natl. Acad. Sci. U.S.A.* **75**, 64–68 (1978).
- Cate, J. H. & Doudna, J. A. *Structure* **4**, 1221–1229 (1996).
- Scott, W. G., Finch, J. T. & Klug, A. *Cell* **81**, 991–1002 (1995).
- Portmann, S., Usman, N. & Egli, M. *Biochemistry* **34**, 7569–7575 (1995).
- Correll, C. C., Freeborn, B., Moore, P. B. & Steitz, T. A. *Cell* **91**, 705–712 (1997).
- Deslongchamps, P. *Stereoelectronic effects in organic chemistry* (Tetrahedron Organic Chemistry Series, Pergamon, Oxford; 1983).
- Cummins, L. L. et al. *Nucleic Acids Res.* **23**, 2019–2024 (1995).
- Tereshko, V. et al. *Biochemistry* **37**, 10626–10634 (1998).
- Lind, K. E., Mohan, V., Manoharan, M. & Ferguson, D. M. *Nucleic Acids Res.* **26**, 3694–3699 (1998).
- Egli, M., Portmann, S. & Usman, N. *Biochemistry* **35**, 8489–8494 (1996).
- Schneider, B., Patel, K. & Berman, H. M. *Biophys. J.* **75**, 2422–2434 (1998).
- Khatsenko, O., Morgan, R. & Geary, R. *Pharm. Res.* **16** in the press (1999).
- Otwinowski, Z. & Minor, W. *Methods Enzymol.* **276**, 307–326 (1997).
- Navaza, J. *Acta Crystallogr. A* **50**, 157–163 (1994).
- Brünger, A. T. *X-PLOR 3.1, A system for X-ray crystallography and NMR* (Yale University Press, New Haven, Connecticut; 1993).
- Parkinson, G., Vojtechovsky, J., Clowney, L., Brünger, A. T. & Berman, H. M. *Acta Crystallogr. D* **52**, 57–64 (1996).
- Marky, L. A. & Breslauer, K. J. *Biopolymers* **26**, 1601–1620 (1987).
- Lavery, R. & Sklenar, H. J. *J. Biomol. Struct. Dyn.* **6**, 655–667 (1989).
- Brünger, A. T. *Nature* **355**, 472–475 (1992).